LASER INTERFEROMETER GRAVITATIONAL WAVE OBSERVATORY
- LIGO -
CALIFORNIA INSTITUTE OF TECHNOLOGY
MASSACHUSETTS INSTITUTE OF TECHNOLOGY

Technical Note	**LIGO-T26xxxxx–**	2026/09/24

Final Report: A Physics-Accurate Digital Twin and System Identification Framework for the Caltech 40 m Prototype Input Mode Cleaner

Arush Pimpalkar

California Institute of Technology
LIGO Project, MC100-36
Pasadena, CA 91125
Phone (626) 395-2129
Fax (626) 304-9834
E-mail: info@ligo.caltech.edu

Massachusetts Institute of Technology
LIGO Project, Room NW22-295
Cambridge, MA 02139
Phone (617) 253-4824
Fax (617) 253-7014
E-mail: info@ligo.mit.edu

LIGO Hanford Observatory
Route 10, Mile Marker 2
Richland, WA 99352
Phone (509) 372-8106
Fax (509) 372-8137
E-mail: info@ligo.caltech.edu

LIGO Livingston Observatory
19100 LIGO Lane
Livingston, LA 70754
Phone (225) 686-3100
Fax (225) 686-7189
E-mail: info@ligo.caltech.edu

http://www.ligo.caltech.edu/

Contents

1 Introduction **2**

2 Closed-Loop Length Control **4**

2.1 Stability assessment 4

2.2 Loop design and result 5

3 Completing the Angular Sensing Model **6**

3.1 A third angular sensor 6

3.2 Choice of the yaw beam-spot matrix 7

3.3 Absolute WFS amplitude and shot-noise floor 7

4 Closed-Loop Angular (ASC) Control **7**

4.1 Loop structure 7

4.2 Result 8

5 Unified Full-IMC Lock **9**

5.1 All three loops closed together 9

5.2 Length and angular decoupling 9

5.3 Transmitted-power lock indicator 9

6 Validation Against 40 m Measurements **9**

6.1 Angular sensing: dither campaign (cavity locked) 10

6.2 Length signals: free-swinging scans (cavity unlocked) 11

7 Challenges and Open Problems **12**

8 Modelling Assumptions **13**

9 Conclusions and Future Work **14**

Abstract

This report presents the completed digital twin of the Caltech 40 m Prototype Input Mode Cleaner (IMC), an isosceles triangular three-mirror suspended cavity. The twin combines a seismically driven model of the three mirror suspensions, a linear optical model of the cavity, and all three control loops of the real instrument: the Pound–Drever–Hall (PDH) length loop actuated on MC2 and the pitch and yaw alignment (ASC) loops driven by two wavefront sensors (WFS) and a beam-centering quadrant photodiode (QPD) on the MC2 transmission. Both loops use servo filter shapes read from the 40 m FOTON files and, for ASC, the engaged filter modules recorded in a front-end snapshot. Because the open loops contain marginal poles, the classical Bode margins are unreliable, and stability is established with a time-domain test. With the real inverse-plant controller the length loop crosses at 3 Hz and suppresses the seismic round-trip length fluctuation from 1.40 µm to 0.40 µm RMS. The ASC loops cross near 1 Hz, suppress slow angular drift, and leave the seismic band to the local damping. The three loops run together stably, and length and angle are decoupled exactly to first order. The WFS response was placed on an absolute scale (W/rad) and a calibration-free shot-noise floor was derived, showing that the IMC alignment is seismic-limited by roughly seven orders of magnitude. The sensing model was compared with a dither campaign on the 40 m: all 18 sensor-mirror couplings predicted as non-zero were detected with the predicted sign, using the yaw beam-spot matrix of Eq. 37 of the reference model and WFS readout phases fitted to the data. A preliminary, still incomplete analysis of free-swinging cavity scans reproduces the shape of the PDH error signal. The remaining gaps, chiefly the electronics and actuator calibrations and unmodelled pitch-yaw cross-coupling seen in the data, are listed with the next steps.

1 Introduction

The Laser Interferometer Gravitational-Wave Observatory (LIGO) relies on suspended optics and active control to keep its interferometers aligned and on resonance. At the lowest frequencies of the detection band the sensitivity is limited by the control noise these loops inject onto the mirrors [1], so the design of the loops bounds the astrophysical reach of the instrument. The Caltech 40 m Prototype shares the optical topology and control problems of the full detectors and serves as a testbed for control schemes intended for the observatories [2]. Its Input Mode Cleaner is a triangular cavity formed by two flat mirrors (MC1, MC3) on the short side and a curved apex mirror (MC2), which filters the laser in spatial mode, polarization and frequency before it enters the main interferometer.

The goal of this project is a validated digital twin of the IMC that can be used to develop and test controllers without touching the locked hardware, with the downstream aim of training a Deep Loop Shaping reinforcement-learning controller [1] against an ensemble of validated models. The twin has three parts. The *mechanical* model propagates ground motion measured by the STS-2 seismometers through the isolation stack (LIGO T000058) [5] and the single-stage pendulum response (LIGO T000134) [4] to each mirror, where a discrete-time OSEM local damping loop reduces the free suspension resonance from $Q \approx 10^4$ to $Q \approx 5.5$. It runs as three instances (MC1, MC2, MC3) that share the pendulum and seismic path but use each mirror's own sensor and servo filters from the 40 m FOTON files, and it

was checked against measured transfer functions of the 40 m local damping loop. The *optical* model is the linear response of the triangular cavity to mirror motion, following the method of Tanioka *et al.* [3], with a Pound–Drever–Hall (PDH) length sensor [6], and it is cross-checked against the independent encoding of the same cavity in the Andric 2022 thesis [7]. The *integration* stage closes the cavity control loops and compares the result with 40 m data.

Figure 1 shows the sensing and control layout that the final twin reproduces. A suspended mirror is a rigid body with six degrees of freedom: three translations (longitudinal, side, vertical) and three rotations (pitch, yaw, roll). The twin models only the longitudinal (L), pitch (P) and yaw (Y) motion of each mirror. These are the degrees of freedom that change the cavity length and the direction of the optical axis to first order, and they are the ones sensed and controlled by the IMC loops and damped by the OSEM loops. Side, vertical and roll motion couple to the cavity only weakly and are neglected. The beam reflected from MC1 is split between the PDH length sensor, which produces the length error signal, and the two WFS heads, which sense angular misalignment; a DC QPD on the MC2 transmission provides the third angular sensor and the transmitted power (MC-TRANS) used as the lock indicator.

The report describes the length loop (Section 2), the angular sensing model (Section 3), the closed ASC loops (Section 4), and the unified lock with all three loops closed (Section 5). Section 6 compares the model with measurements taken on the 40 m, and the remaining sections collect the open problems, the modelling assumptions and the future work.

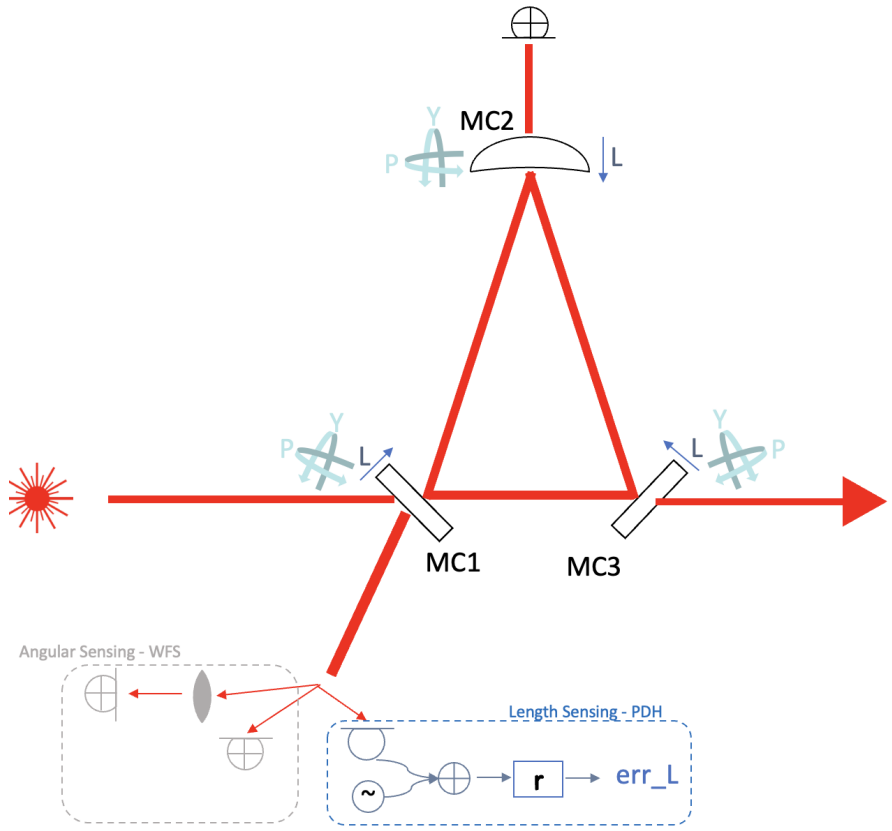


Figure 1: Sensing layout of the 40 m IMC reproduced by the twin. The laser enters through the flat mirror MC1, circulates via the curved apex mirror MC2, and leaves through the flat mirror MC3. For each mirror the twin models the longitudinal (L), pitch (P) and yaw (Y) degrees of freedom, the three that couple to the cavity at first order. The beam reflected by MC1 feeds the angular sensing (the two wavefront sensors) and the PDH length sensing, where the photodiode signal is demodulated with the RF local oscillator and filtered to give the length error signal err_L. The quadrant photodiode on the MC2 transmission completes the angular sensor set and provides the transmitted power used to detect lock.

2 Closed-Loop Length Control

2.1 Stability assessment

The Bode criterion for phase and gain margins assumes that the open loop is strictly stable. That assumption does not hold for the IMC loops: the OSEM-damped plant has a pole at $|z| \approx 0.9999995$, essentially on the unit circle, and a servo containing an integrator adds another. In this situation the Bode margins can be misleading. For example, a simple servo made of an integrator boost and a 55 Hz roll-off shows a unity-gain frequency (UGF) of 50 Hz with 78° phase margin, yet the closed loop is unstable. Stability in the twin is therefore decided by a direct time-domain test, which propagates an impulse around the discrete-time loop and checks whether it decays. This test is applied to every loop in the report, and a regression test checks that it flags the unstable example above.

2.2 Loop design and result

The length loop feeds the PDH error signal back to the longitudinal actuator of MC2. Its open-loop gain is the product of four parts:

$$L(s) = \underbrace{K_0}_{\text{gain}} \underbrace{D_L \frac{1}{1 + s/\omega_p}}_{\text{PDH sensing}} \underbrace{K_{\mathrm{MCL}}(s)}_{\text{servo}} \underbrace{2\, H_{\mathrm{susp}}(s)}_{\text{MC2 motion}}. \tag{1}$$

The PDH sensor converts length into signal with slope $D_L \approx -5.85 \times 10^8\,\mathrm{W\,m^{-1}}$ and a cavity pole at 3.78 kHz. The servo is the filter set used on the 40 m: an inverse-plant filter, the length controller, and a 55 Hz roll-off. The plant H_{susp} is the MC2 suspension with its local damping loop closed (Fig. 2); this suspension model agrees with the measured damping loop on MC3 (Fig. 3). The factor 2 converts MC2 displacement into round-trip length. The overall gain K_0 stands in for the calibrations that have not been measured, and is set to place the unity-gain frequency.

The loop crosses at 3 Hz with 39° phase margin and is stable in the time-domain test; above about 5 Hz it becomes unstable. It reduces the seismic round-trip length fluctuation from 1.40 µm to 0.40 µm RMS, a factor of about 3.5. A longitudinal kick on a single mirror gives the same picture: the length loop reduces the ring-down by a factor of 3.3 for MC1, 3.4 for MC2 and 3.3 for MC3.

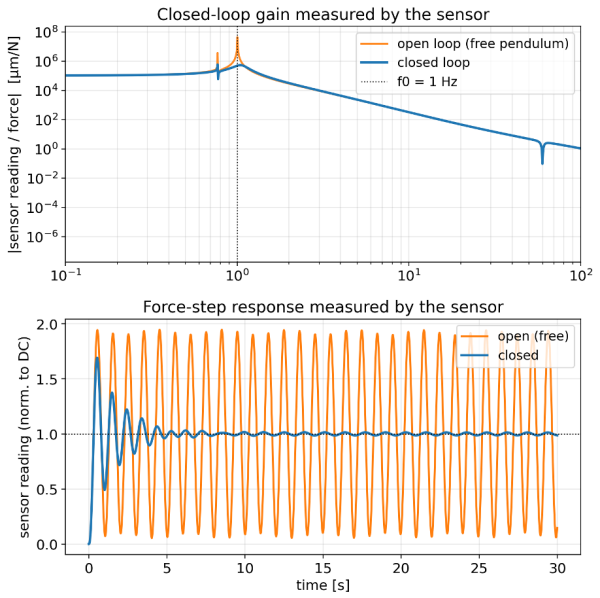


Figure 2: Longitudinal response of a suspended mirror with the OSEM local damping loop, which forms the actuation plant of the length loop. Top: sensor reading per unit force for the free pendulum (open loop) and with local damping (closed loop); the damping loop removes the sharp resonance at $f_0 = 1\,\mathrm{Hz}$. Bottom: response to a force step, normalised to its DC value; the free pendulum keeps ringing, while the damped suspension settles within a few seconds.

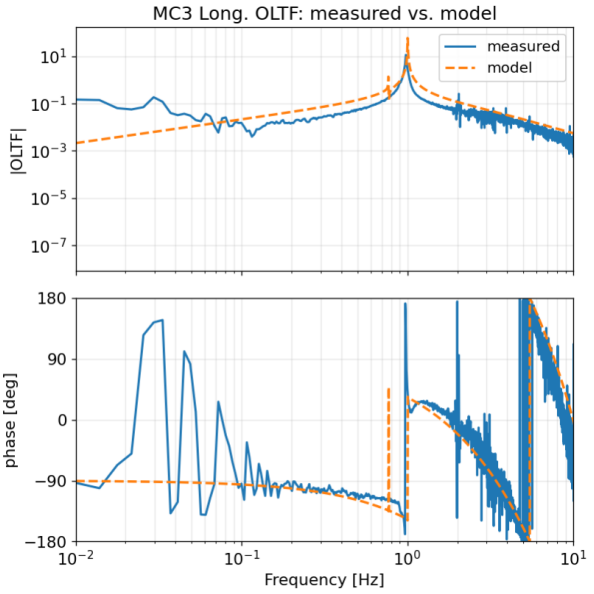


Figure 3: Open-loop transfer function of the MC3 longitudinal damping loop, measured on the 40 m (solid) and predicted by the suspension model (dashed), in magnitude (top) and phase (bottom). The model follows the measurement from about 0.2 Hz to 10 Hz, through the 1 Hz resonance. Below about 0.1 Hz the measurement departs from the model; there the excitation does not stand well above the natural motion of the suspension, and the measurement is not reliable.

3 Completing the Angular Sensing Model

3.1 A third angular sensor

The two WFS heads give a 2×3 sensing matrix of rank 2 for each of pitch and yaw: they measure the tilt and translation of the cavity waist but are blind to the mirror combinations $[1, -\sqrt{2}\,g, 1]$ (pitch) and $[1, 2g, 1]$ (yaw) [3]. A three-mirror loop cannot be closed on a rank-2 sensor set, because the null combination cannot be controlled. The twin therefore adds the DC beam-centering QPD on the MC2 transmission, which the 40 m also uses. Its response has a non-zero projection on the WFS null direction, and the stacked 3×3 sensing matrix is full rank for both degrees of freedom (the same sensor set used in the Andric thesis [7]).

The QPD is not on the MC2 surface. It reads the beam centroid at MC2 plus the transmitted beam angle multiplied by the path length d from MC2 to the detector:

$$q = p\left[B_{\mathrm{MC2}} + \frac{d}{L}\left(B_{\mathrm{MC2}} - B_{\mathrm{MC1}}\right)\right], \tag{2}$$

where B is the beam-spot matrix row for each mirror, L is the long arm length, and $p = \pm 1$ is the image parity of the transmission path. The path length was measured on the 40 m table

as $d = 0.70\,\mathrm{m}$ (60 cm from MC2 to a fold mirror and 10 cm from the fold to the photodiode). The single horizontal fold inverts the image in yaw only, so $p = +1$ for pitch and $p = -1$ for yaw. Because this parity cannot be separated from the QPD quadrant wiring convention, it is treated as a calibrated sign, and only the ratios within a QPD row are convention-free tests of the model.

3.2 Choice of the yaw beam-spot matrix

For yaw, Eqs. 37 and 40 of Tanioka *et al.* are not consistent with each other: Eq. 37, the on-mirror beam-spot matrix, implies that the waist translation couples to the MC2 angle, whereas Eq. 40 says it couples only to the differential angle of the two flat mirrors. A beam-spot matrix reconstructed from Eq. 40 has the two flat mirrors interchanged relative to Eq. 37, which swaps the MC1 and MC3 entries of the QPD yaw row. The 40 m measurement (Section 6) decides between the two: the measured signs of the QPD yaw ratios MC1/MC2 (negative) and MC3/MC2 (positive), which do not depend on any readout convention, are reproduced with Eq. 37 and the measured lever arm, and inverted with the Eq. 40 form. The twin therefore uses the matrix of Eq. 37, transcribed directly from the paper. The yaw WFS matrix (Eq. 49) is independent of this choice.

3.3 Absolute WFS amplitude and shot-noise floor

The WFS matrices of Tanioka *et al.* are given in dimensionless units. The missing factor for an absolute scale is the per-mirror normalized-angle coefficient $2\pi w(z_i)/\lambda$ (their Eq. 11), which depends on the beam size at each mirror. With it, the WFS response is expressed in W/rad by multiplying the validated sensing matrices by $P_0 J_0(m) J_1(m) G_{00}\,(2\pi/\lambda)$, giving a scale of $1.47 \times 10^8\,\mathrm{W\,m^{-1}\,rad^{-1}}$ for the 40 m parameters ($P_0 = 1\,\mathrm{W}$, modulation depth $m = 0.1$). The geometry, readout quadratures and rank-2 null are unchanged; only the amplitude is added.

The DC powers at the readout ports are 4.99 mW at the WFS (dominated by the reflected sidebands) and 4.95 mW at the MC2-transmission QPD, giving a WFS shot noise of $\sqrt{2h\nu P_{\mathrm{DC}}} \approx 6.1 \times 10^{-11}\,\mathrm{W}/\sqrt{\mathrm{Hz}}$. Referred to mirror angle through the inverse of the absolute three-sensor matrix, the readout floor is about $1.5 \times 10^{-12}\,\mathrm{rad}/\sqrt{\mathrm{Hz}}$ for MC1 and MC3 and $6 \times 10^{-13}\,\mathrm{rad}/\sqrt{\mathrm{Hz}}$ for MC2 in pitch, with similar values in yaw. The watts cancel in this ratio, so the floor needs no photodiode, ADC or coil calibration. An O(1) factor remains in the conversion from the demodulated signal of Eq. 44 to physical photodiode power (reflection-port coupling and QPD mode overlap), and there is no published numerical anchor for the 40 m geometry; this factor is stated rather than fitted.

4 Closed-Loop Angular (ASC) Control

4.1 Loop structure

The ASC loop runs from the three-sensor stack (WFS1, WFS2 and the MC2 QPD) through the servo and an output matrix to torques on the three mirrors, which act on the OSEM-

damped pitch and yaw responses. The output matrix is the inverse of the (row-normalised) sensing matrix. Because the three suspensions share the same angular response $H(\omega)$, the 3×3 open loop reduces to

$$L_{\mathrm{mat}}(\omega) = S\, H(\omega)\, K(\omega)\, S^{-1} = L(\omega)\, I_3, \tag{3}$$

so the multi-input loop decouples into three identical single-input loops. Numerically the off-diagonal residual is 3×10^{-14} in pitch and 4×10^{-14} in yaw. A useful consequence is that the unknown overall WFS calibration cancels between S and S^{-1}, so the loop shape does not depend on it.

The servo is the real 40 m IMC WFS servo from the IMC front-end model, with the engaged filters read from a front-end snapshot: a low-frequency boost, a second low-frequency gain stage, a roll-off and a lead compensator. The low-frequency boost is essential: the suspension-side angular conditioning filters on MC2 have no low-frequency gain, and a loop built on them alone is only conditionally stable. The overall gain K_0 is a single swept scalar chosen for a target UGF of 0.8 Hz, consistent with the 0.5–1 Hz bandwidth of the 40 m WFS loops. The output matrix is the ideal inverse rather than the measured 40 m matrix, by design.

4.2 Result

Both loops are stable in the time-domain test. The pitch loop crosses at 0.80 Hz with $M_s = 5.3$ dB ($K_0 = 7.77 \times 10^{-3}\,\mathrm{N\,m\,rad^{-1}}$) and the yaw loop at 0.96 Hz with $M_s = 6.5$ dB ($K_0 = 8.83 \times 10^{-2}\,\mathrm{N\,m\,rad^{-1}}$). The Bode phase margins are not quoted, for the reason given in Section 2.

The ASC loop has a specific role. It suppresses slow angular drift, by a factor of 8 at 0.01 Hz, which is the purpose of the WFS servo. It does not suppress the seismic band around the pendulum resonances, where the servo gain is low and the OSEM damping already acts: the pitch residual angle changes from 24.7 µrad to 28.7 µrad RMS, and the beam-walk RMS on MC2 from 625 µm to 725 µm (MC1 and MC3: 461 µm to 535 µm). The yaw seismic budget is zero because the available ground data are translational only and yaw is a pure torsion mode; this is flagged rather than filled with an assumed input.

The closed loop also imprints the sensor noise on the mirrors below the UGF. The injected WFS shot noise gives a pitch residual of about 4×10^{-13} rad RMS on MC2 and 1×10^{-12} rad on MC1 and MC3, a factor of about 3.5×10^{-8} below the seismic residual. The IMC alignment is therefore seismic-limited, with ample margin before shot noise matters.

With the optical response on an absolute scale, K_0 separates into the pinned optical gain and an electronics-plus-coil factor (photodiode and ADC counts per watt times coil torque per count). The model gives this remaining factor as $3.0 \times 10^{-8}\,\mathrm{N\,m\,W^{-1}}$ for pitch and $3.5 \times 10^{-7}\,\mathrm{N\,m\,W^{-1}}$ for yaw; it is the part that still needs a 40 m calibration.

5 Unified Full-IMC Lock

5.1 All three loops closed together

The length loop and the two ASC loops were run together on a common time base, each with its impulse response computed by the same discrete-time engine used for the stability tests. All three decay, so the combined lock is stable. The ratio of late to early impulse-response amplitude, which is below one for a decaying response, is 0.12 for the length loop, 0.22 for ASC pitch and 0.11 for ASC yaw. The loops cross at 3.00 Hz (length), 0.80 Hz (pitch) and 0.96 Hz (yaw), with peak sensitivities of 7.4, 5.3 and 6.5 dB respectively.

5.2 Length and angular decoupling

The length bandwidth is only about three times the ASC bandwidth, so the loops overlap in frequency and band separation cannot be relied on to keep them independent. The decoupling in the twin is structural. The length and angular loops act on orthogonal suspension degrees of freedom of MC2, each with its own plant, and the PDH signal has no first-order response to mirror tilt, because a tilt excites the TEM_{01} or TEM_{10} mode, which is orthogonal to the TEM_{00} carrier read by PDH. The first-order angle-to-length coupling is therefore exactly zero. The impulse responses make this visible: an angular kick on any mirror produces pitch and yaw ring-downs and an identically zero length readout. The ASC loop changes the ring-down quality factor only slightly (pitch 4.0 to 4.2, yaw 5.0 to 4.5), as expected for a slow alignment loop.

The leading coupling is second order (angle squared to length, through beam walk and mode overlap). A simple geometric estimate of ~ 10 nm at the residual beam walk overestimates the effect on the controlled cavity length, because the cavity eigenmode re-centres on the tilted axis, so it is not used as a bound. A reliable value requires a modal optics model (Finesse or Optickle) and is left as future work.

5.3 Transmitted-power lock indicator

A DC power monitor on the MC2 transmission (MC-TRANS) was added as the lock-acquisition signal. It reads the carrier buildup transmitted through MC2, with a peak of 4.95 mW on resonance for 1 W input, the same DC power seen by the beam-centering QPD on that port. Using half of the peak as the lock threshold gives a capture window of ± 3.78 kHz in laser detuning, equal to half the 7.55 kHz linewidth, which corresponds to ± 170 pm of MC2 motion and ± 240 pm of MC1 or MC3 motion. The monitor is not part of any feedback loop; the length lock uses the reflected PDH signal. Its counts-per-watt calibration is not yet measured, so it reports physical watts.

6 Validation Against 40 m Measurements

Two classes of measurement were taken on the 40 m: the angular sensing response with the cavity locked, and the length signals with the cavity unlocked.

6.1 Angular sensing: dither campaign (cavity locked)

Method. Each of the six mirror angular degrees of freedom (MC1, MC2, MC3 in pitch and yaw) was driven in turn with a 10 Hz sine through its calibration excitation point, at amplitudes of 12.4, 124, 372 and 744 counts, and the six angular sensor outputs were recorded: the pitch and yaw signals of WFS1, WFS2 and the MC2-transmission QPD. The analysis below uses the 744-count, 1 s (10-cycle) records, with the 372-count set as a consistency check. For each of the 36 sensor-excitation cells the coupling is the in-phase matched-filter slope of the sensor response against the excitation. Whether the 10 Hz line is present in a cell was decided with a harmonic F-test against the neighbouring spectrum, with the Benjamini–Hochberg false-discovery-rate correction [8] over the 36 cells; a cell counts as detected for $q < 0.05$. No counts-to-radian actuator calibration exists yet, so the slopes are in counts per count and only signs and ratios can be compared with the model.

Readout parameters. Three readout conventions are not predicted by the reduced model and were set from the measurements. The WFS readout Gouy phases were fitted as $\eta_1 = -18°$ and $\eta_2 = 47°$ (separation 65°). A symmetric pair of phases forces two mirror-image cells (WFS1 yaw from MC1 and WFS2 yaw from MC3) to the same sign, whereas the data give them opposite signs; with a symmetric $\pm 35°$ and unit head polarities only 5 of the 12 WFS sign cells agree. An unconstrained fit gives $(-16.25°, 46.25°)$, consistent with the measured 65–70° separation band. The overall pitch polarity of both WFS heads was set to -1, since both measured pitch rows are exact sign negations of the model rows, which no choice of Gouy phases can reproduce. The QPD parity is set by the fold geometry as described in Section 3.

Results. Figure 4 compares the signs. All 18 cells that the model predicts to be non-zero are detected with high significance, and all 18 have the predicted sign (12 WFS cells and 6 QPD cells). Because the Gouy phases and polarities above were chosen using these data, the WFS sign agreement is a consistency check rather than an independent prediction. The QPD yaw row is a sharper test: the signs of its ratios do not depend on any convention, and they are reproduced only with the Eq. 37 beam-spot matrix and the measured lever arm. The measurements also confirm that MC2 produces the largest response in every sensor channel, as the model predicts.

The comparison also exposes two limitations. First, the magnitudes are not yet matched: after the per-mirror gains are left free, the typical magnitude error is a factor of 1.2 to 1.3, but the model's ratio of flat-mirror to apex-mirror response differs from the data by a factor of 2 to 5, and the pitch and yaw blocks alone prefer different WFS head separations (44° and 85°). Resolving this requires a counts-to-radian calibration of the actuators. Second, 11 of the 18 cells that the linear model predicts to be exactly zero (pitch-yaw cross terms) show a significant line. Most are small, but two are not: WFS1 pitch responds to MC2 yaw with a slope of -0.184, comparable to its response to MC2 pitch, and WFS2 yaw responds to MC2 pitch with $+0.097$. The model has no mechanism for pitch-yaw cross-coupling, so these terms point to a physical effect outside the model, such as actuator cross-coupling on MC2 or a rotation of the sensor heads; the origin has not been identified.

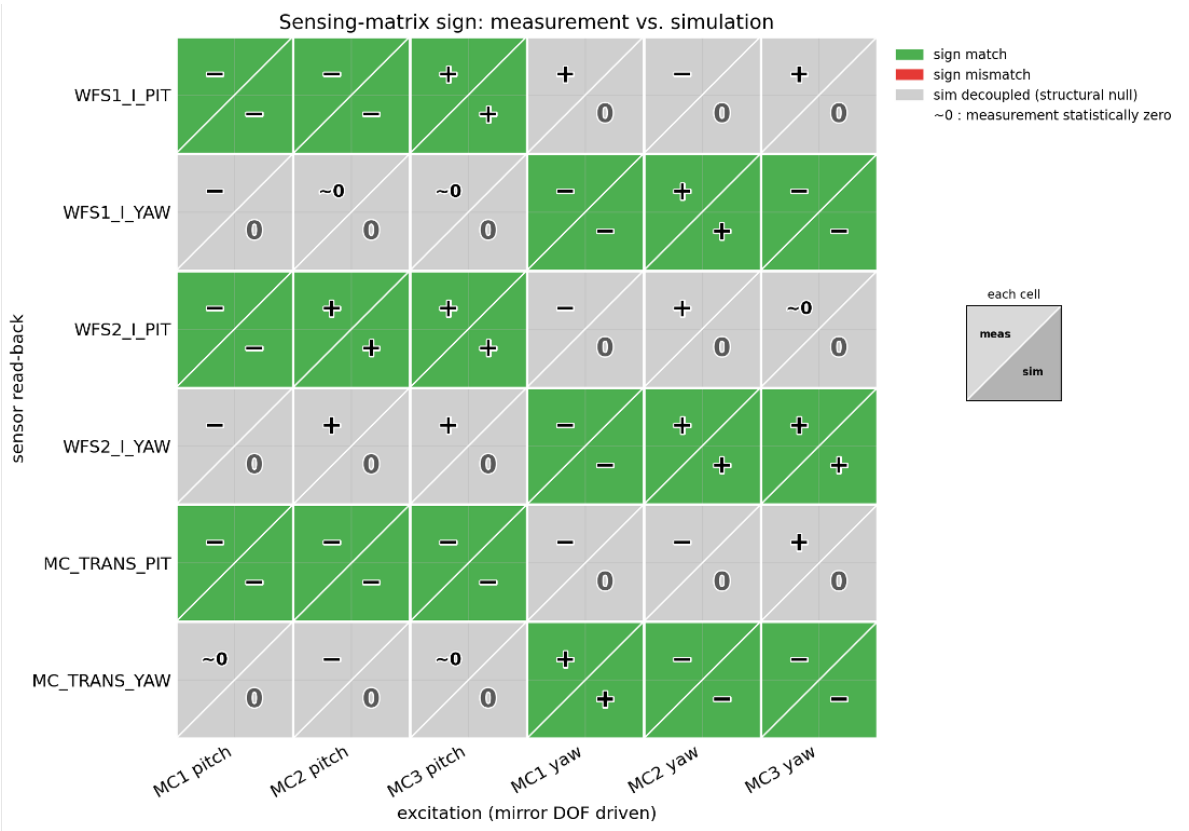


Figure 4: Sign of the sensing matrix, measurement versus simulation. Rows are the sensor outputs (pitch and yaw of WFS1, WFS2 and the MC2-transmission QPD); columns are the driven mirror degree of freedom. Each cell is split diagonally: the upper-left half gives the measured sign and the lower-right half the simulated sign. Green: the model predicts a non-zero coupling and the signs match (18 of 18). Grey: the model predicts a structural null (0). A measured entry of ~ 0 means the measurement is statistically zero.

6.2 Length signals: free-swinging scans (cavity unlocked)

Method. The PDH error and output powers as a function of mirror position cannot be measured with the cavity locked, since the loop holds the length fixed. No displacement was commanded; instead, with ASC off, the input filters disabled and the local damping of one mirror turned off, the free-swinging suspension sweeps the cavity through resonance about once per second. The PDH length error, the DC power transmitted through MC2 and the DC photodiode signal at the reflection port were recorded. The model PDH error was fitted to a clean resonance crossing to convert time into mirror displacement, using the coupling factor of the mirror whose damping was off. The measured powers were scaled to the model peak, since no absolute photodiode calibration is available, so the power comparison tests shape and width only.

Results. This analysis is not yet complete, and the results below are preliminary. For all three mirrors the fitted model reproduces the antisymmetric shape and zero crossing of the measured PDH error, including the opposite sign of the MC3 crossing (Fig. 5). The data

depart from the template in the wings, with flatter extrema and additional structure on either side. For the MC2 crossing (fitted sweep speed 299 nm s^{-1}), the MC2 transmission follows the model width near resonance, but away from resonance it shows secondary fringes that the static model does not contain. The reflection-port DC signal, which was compared with the MC3 transmission model in this analysis, does not follow that model: it stays near 0.3 of its peak far from resonance and dips at the centre. Which cavity port this signal represents, and its normalisation, need to be revisited before it can be used quantitatively.

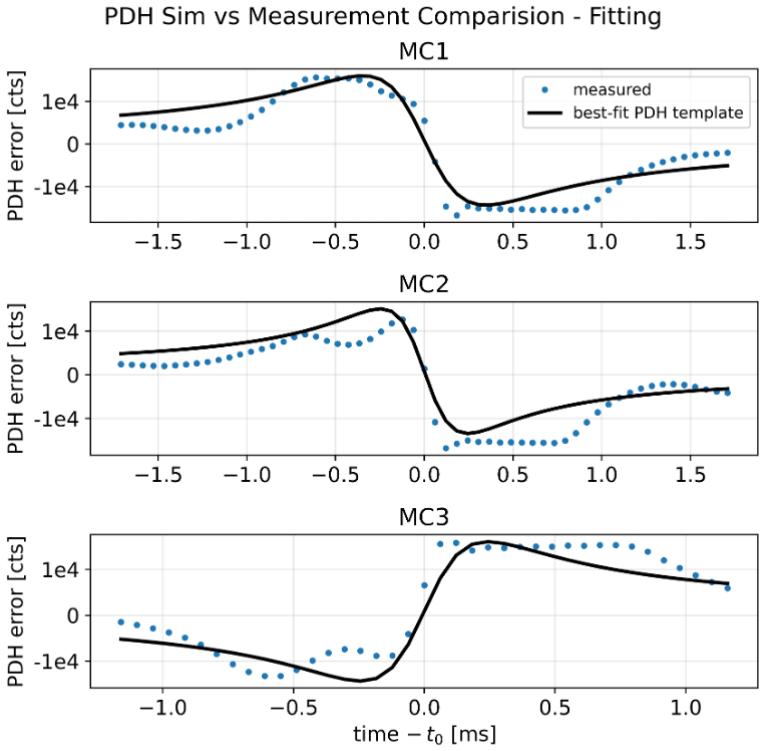


Figure 5: Preliminary verification of the PDH length sensing: measured PDH length error during a free-swinging resonance crossing (points) and the best-fit model template (line), for the crossings with MC1, MC2 and MC3 undamped. The analysis is incomplete.

7 Challenges and Open Problems

- **Bode margins near marginal poles.** The open loops contain poles on or very near the unit circle, which makes the classical margins misleading and can hide an unstable loop. All stability statements rest on the time-domain test; frequency domain margins are reported only as supporting information.
- **Electronics and actuator calibration.** The loop shapes are fixed by measured filters, but the absolute gains are single swept scalars. The optical part of the ASC gain is absolute; the photodiode, ADC and coil factors are not. The counts-to-radian actuator calibration is also what limits the magnitude comparison with the dither data.

- **Unmodelled pitch-yaw coupling.** The dither data show significant pitch-yaw cross terms, two of them large, that the linear model sets to zero.
- **Flat-to-apex response ratio.** The model's ratio of flat-mirror to apex-mirror WFS response differs from the data by a factor of 2 to 5.
- **Inconsistent equations in the reference paper.** Equations 37 and 40 of Tanioka *et al.* disagree for the yaw waist translation; the 40 m data favour Eq. 37, which the twin uses.
- **Suspension-model items.** A lumped 85 ms delay is needed to match the measured phase of the local damping loop, and its origin is not established. The STS-2 instrument-response deconvolution and a dedicated measurement of the OSEM sensor noise are also still open.
- **Code state.** Two regression scripts (`test_full_lock.py` and `test_sensing.py`) do not pass on the current development branch; they still assume MC1/MC3 symmetry in the QPD yaw row, which the Eq. 37 beam-spot matrix and the measured lever arm break, and need to be updated.

8 Modelling Assumptions

- **Linear optics.** The cavity response is the linearised Tanioka model; the optical part is a set of static matrices, and frequency dependence enters only through the suspensions and the cavity pole.
- **Identical suspensions in the cavity loops.** The ASC decoupling is exact only because the three mirrors share one angular response; per-mirror differences would leave residual cross-coupling.
- **Ideal output matrix.** The ASC output matrix is the inverse of the model sensing matrix, not the measured 40 m matrix.
- **Swept loop gains.** Each loop's absolute gain is one scalar chosen for a target UGF (3 Hz length, 0.8 Hz ASC).
- **Slow length path only.** The length loop models the MC2 actuation path; the laser-frequency (FSS) path is not included.
- **Independent mirror disturbances.** Seismic residuals of the three mirrors are combined in quadrature.
- **No rotational ground input.** The yaw seismic budget is zero because only translational ground data are available.
- **Design-optics geometry.** The cavity uses the prototype-upgrade design ($g = 0.2904$), not the as-built 2020 geometry ($g \approx 0.24$) modelled by Andric.

- **Fitted readout conventions.** The WFS Gouy phases, the WFS head polarities and the QPD parity are calibrated from the 40 m measurements rather than predicted.
- **Stated O(1) in the absolute WFS scale.** The reflection-port coupling and QPD mode overlap are set to one.

9 Conclusions and Future Work

The IMC twin is a full model of the locked cavity: three suspension instances with the 40 m damping filters, a linear optical model of the triangular cavity with absolute WFS scaling, a PDH length loop and two ASC loops built on the real 40 m servo filters, and a unified simulation in which all three loops are closed and stable. Two methodological points emerged: stability of these loops must be tested in the time domain, because the Bode criterion can report a stable loop that is not, and the yaw beam-spot matrix must follow Eq. 37 of the reference model, which the 40 m data favour over Eq. 40. Against measurement, the suspension loop matches the 40 m damping loop around resonance, the angular sensing model matches the signs of all 18 detected sensor couplings, and a preliminary, still incomplete analysis indicates that the PDH model reproduces the measured error-signal shape.

The next steps are:

1. Measure the counts-to-radian and counts-to-newton actuator calibrations and the photodiode and ADC gains, and use them to replace the swept loop gains and to compare the WFS magnitudes, not only their signs.
2. Identify the origin of the pitch-yaw cross terms seen in the dither data and of the flat-to-apex magnitude discrepancy, and extend the model accordingly.
3. Complete the free-swinging analysis of the PDH error signal, establish which port the reflection DC signal represents, and repeat the comparison for the output powers with calibrated photodiodes.
4. Add a modal optics model (Finesse or Optickle) to quantify the second-order angle-to-length coupling.
5. Add rotational ground-motion input so that the yaw budget is physical, and resolve the suspension-model items (the 85 ms phase mismatch, the STS-2 deconvolution and the OSEM noise measurement).
6. Update the two failing regression scripts and carry out gray-box system identification [9] against the 40 m data to produce a validated ensemble of twins, which can then be used to train a Deep Loop Shaping controller [1].

References

[1] J. Buchli *et al.*, "Improving cosmological reach of a gravitational wave observatory using Deep Loop Shaping," *Science* **389**, 1012–1017 (2025). DOI: 10.1126/science.adw1291. arXiv:2509.14016.

[2] R. Ward, R. Adhikari *et al.*, "dc readout experiment at the Caltech 40m prototype interferometer," *Class. Quantum Grav.* **25**, 114030 (2008).

[3] S. Tanioka, G.-G. Ge, K. Kokeyama, M. Nakano, J. Park, and K. Izumi, "Angular response of a triangular optical cavity analyzed by a linear approximation method," arXiv:2002.02703 [physics.optics] (2020).

[4] *Pendulum response of a single-stage suspension*, LIGO Document T000134. https://dcc.ligo.org/T000134.

[5] *Horizontal seismic isolation stack characterisation*, LIGO Document T000058. https://dcc.ligo.org/T000058.

[6] E. D. Black, "An introduction to Pound–Drever–Hall laser frequency stabilization," *Am. J. Phys.* **69**, 79–87 (2001). DOI: 10.1119/1.1286663.

[7] T. Andric, *Low-frequency sensitivity limitations in current and future gravitational-wave detectors*, Doctoral thesis, Gran Sasso Science Institute (2022). https://iris.gssi.it/retrieve/2d7f13e1-b807-4861-9414-b949aa2f67e6/2023_PhDThesis_Andric.pdf.

[8] Y. Benjamini and Y. Hochberg, "Controlling the false discovery rate: a practical and powerful approach to multiple testing," *J. R. Stat. Soc. B* **57**, 289–300 (1995).

[9] L. Ljung, *System Identification: Theory for the User*, 2nd ed., Prentice Hall (1999).